Contact-mediated cellular communication supplements positional information to regulate spatial patterning during development

Chandrashekar Kuyyamudi,[1,2] Shakti N. Menon,[1] and Sitabhra Sinha[1,2]
[1]*The Institute of Mathematical Sciences, CIT Campus, Taramani, Chennai 600113, India*
[2]*Homi Bhabha National Institute, Anushaktinagar, Mumbai 400 094, India*

(Received 11 February 2021; revised 21 May 2021; accepted 2 June 2021; published 21 June 2021)

Development in multicellular organisms is marked by a high degree of spatial organization of the cells attaining distinct fates in the embryo. Recent experiments showing that suppression of intercellular interactions can alter the spatial patterns arising during development suggest that cell fates cannot be determined by the exclusive regulation of differential gene expression by morphogen gradients (the conventional view encapsulated in the French flag model). Using a mathematical model that describes the receptor-ligand interaction between cells in close physical proximity, we show that such intercellular signaling can regulate the process of selective gene expression within each cell, allowing information from the cellular neighborhood to influence the process by which the thresholds of morphogen concentration that dictate cell fates adaptively emerge. This results in local modulations of the positional cues provided by the global field set up by the morphogen, allowing interaction-mediated self-organized pattern formation to complement boundary-organized mechanisms in the context of development.

DOI: 10.1103/PhysRevE.103.062409

Spatial symmetry breaking is a fundamental prerequisite to morphogenesis, or the development of form, in living organisms, such that an initially homogeneous domain exhibits patterns in the concentrations of molecular species referred to as morphogens [1–4]. This can come about through either self-organizing reaction-diffusion processes [5–7] or from the anisotropy associated with the concentration gradient of a morphogen produced by a localized source [8–10]. While in the simplest scenario involving the latter mechanism, the morphogen diffuses through space subject to uniform linear degradation [11–15], more complex mechanisms for establishing a morphogen gradient have been proposed [16–21]. Cells attain different fates according to the positional information provided by the local concentration of the morphogen vis-a-vis threshold values that emerge from the dynamics of the interpretation module of their genetic regulatory network [22–25]. However, the spatial pattern of cell fates is not entirely determined by these local interactions as recent experiments have highlighted the role of cell-cell communication in this process [26].

Cells in the developing embryo are known to interact with other cells that are in close physical proximity through contact-mediated signaling. This can occur through binding between membrane-bound receptors and ligands on the surfaces of neighboring cells, a prominent example being the evolutionarily conserved Notch signaling pathway [27]. Notch-mediated interactions, which are believed to have arisen early in evolution, have been shown to play a crucial role in the development of all metazoans [27,28]. It has been demonstrated to help sharpen the boundaries between regions having different cell fates in the presence of fluctuating morphogen concentrations [29], providing an important mechanism for systems to be robust with respect to noisy signals [30–33]. More importantly, Notch signaling is capable of self-regulation as the signaling between neighboring cells implements an effective feedback loop [34].

In this paper we present a plausible mechanistic basis for explaining how intercellular interactions influence cell fate determination, as indicated by recent experiments, e.g., on the mouse ventral spinal cord [26], by allowing Notch to alter the expression of genes in the morphogen interpretation module, which in turn control the production of Notch ligands. Using a three-gene interpretation module associated with the Sonic hedgehog (Shh) morphogen gradient in vertebrate neural tubes [35–37], we show that specific types of Notch-mediated coupling allow the size of the domains corresponding to different cell fates to be varied in a regulated manner. They retain the broad features of the reference pattern obtained in the absence of any intercellular coupling, while avoiding phenotypes that do not preserve the number and the sequence of these domains [Fig. 1(a)]. Our results suggest that the emergent thresholds for the morphogen concentration that determine the localization of various cell fates are not only an outcome of the interaction between the morphogen gradient manifested across an entire embryonic segment with the gene circuit dynamics at the cellular level, but also the intermediate-scale dynamics of intercellular interactions [38].

To investigate how the spatial patterning of cell fates are affected by juxtacrine signaling, we consider a linear array of cells responding to a morphogen whose concentration decays exponentially away from the source [11,39]. This spatial profile is reflected in the response of the cells in terms of the concentration of the downstream signaling molecules released as a result of binding of morphogen molecules to receptors on

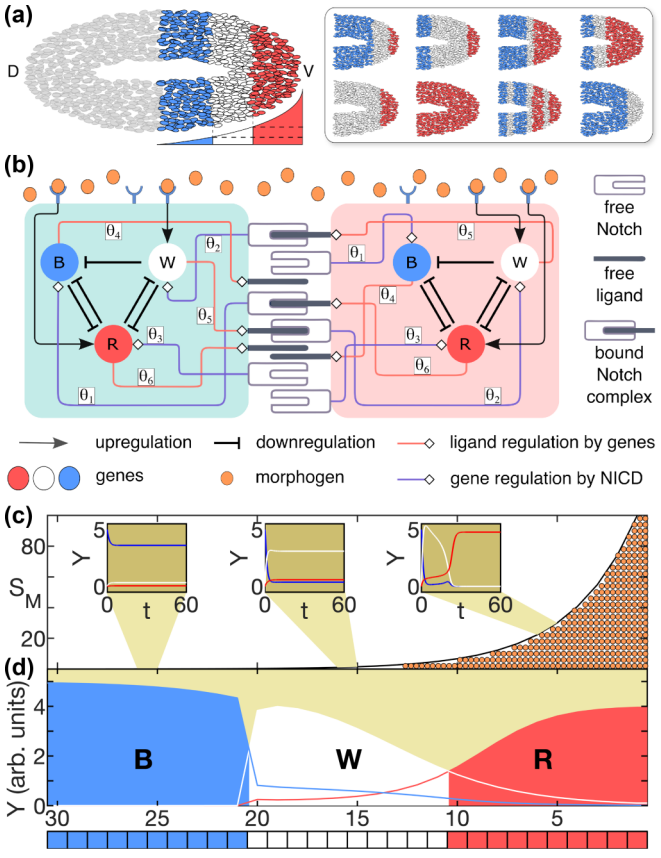

FIG. 1. Contact-mediated signaling regulates the differential expression of cell fates dictated by morphogen concentration profiles. (a) Schematic diagrams illustrating the French Flag problem, namely, how positional information provided by spatial gradients of morphogen concentration specify patterns of cell fates in embryonic tissue. Equally sized domains of cells exhibiting one of three different fates, viz., blue, white, and red, characterize the idealized situation (left), shown for the case of patterning in the ventral region (V) of the vertebrate neural tube by a gradient of Sonic hedgehog morphogen (whose concentration profile is displayed). Under different conditions, variations preserving the chromatic order and number of fate boundaries of the idealized situation can arise (a: right, top row); however, other variations may violate these (a: right, bottom row). (b) Schematic diagram of a pair of cells coupled via Notch signaling in the presence of an external morphogen. Each cell contains a morphogen interpretation module comprising a regulatory circuit of fate-inducing genes B, W, and R. Notch intracellular domains (NICD), released upon successful binding of Notch receptors to ligands from the neighboring cell, affect expression of B, W, and R with strengths $\theta_{1,2,3}$, respectively. This in turn regulates the production of Notch ligand with strengths $\theta_{4,5,6}$. (c) Spatial variation of the response to the morphogen S_M across a one-dimensional domain comprising 30 cells. The three insets display the time evolution of gene expression levels Y ($= B$, W, or R, in arbitrary units) for cells that are subject to low, intermediate, and high morphogen concentrations, respectively. (d) The resulting final expression levels Y of the patterning genes. The maximally expressed gene at each cell determines its fate, as shown in the schematic representation of the 1D domain displayed at the bottom.

the cell membrane, viz., $S_M(x) = S_M(0)\exp(-x/\lambda_M)$, where x is the distance of a cell from the source of the morphogen. The external signal concentration sensed by each cell through its receptors affects the expression of a set of genes that functions as the morphogen interpretation module. We choose one that has been proposed in the context of patterning in the ventral region of the vertebrate neural tube, comprising the genes Pax6, Olig2, and Nkx2.2, in the presence of a Sonic hedgehog (Shh) morphogen gradient [37]. Figure 1(b) shows the module with the regulatory motif of three patterning genes B, W, and R, that mutually repress each other, with the sole exception of W by B. The gene having the highest expression level in each cell determines its fate, indicated by blue, white, or red, which correspond to genes B, W, and R, respectively [Figs. 1(c) and 1(d)]. As Pax6 is the only one of the three genes whose expression occurs even in the absence of the Shh morphogen, we consider this pre-patterning gene (B) to be expressed at very high levels initially, in contrast to the genes Olig2 and Nkx2.2 (represented by W and R, respectively). The time evolution of the expression of the three genes are described by

$$\frac{dB}{dt} = \frac{\alpha + \varphi_1 \frac{N^b}{K_N}}{1 + \left(\frac{R}{K}\right)^{h_1} + \left(\frac{W}{K}\right)^{h_2} + \xi_1 \frac{N^b}{K_N}} - k_1 B, \tag{1}$$

$$\frac{dW}{dt} = \frac{\beta S_M + \varphi_2 \frac{N^b}{K_N}}{1 + S_M + \xi_2 \frac{N^b}{K_N}} \frac{1}{1 + \left(\frac{R}{K}\right)^{h_3}} - k_2 W, \tag{2}$$

$$\frac{dR}{dt} = \frac{\gamma S_M + \varphi_3 \frac{N^b}{K_N}}{1 + S_M + \xi_3 \frac{N^b}{K_N}} \frac{1}{1 + \left(\frac{B}{K}\right)^{h_4} + \left(\frac{W}{K}\right)^{h_5}} - k_3 R, \tag{3}$$

where α, β, γ are the maximum growth rates and $k_{1,2,3}$ are the decay rates of expression for the three genes, while K, K_N, and $h_{1,2,3,4,5}$ specify the nature of the response functions. The parameters $\varphi_{1,2,3}$ and $\xi_{1,2,3}$ are associated with the juxtacrine coupling of adjacent cells through the canonical Notch signaling pathway [27,28]. To describe the dynamics resulting from the coupling, Eqs. (1) to (3) are augmented with the time-evolution equations of the concentrations L and N^b of the Notch ligand and the Notch intracellular domain (NICD), respectively,

$$\frac{dL}{dt} = \frac{\beta_L + \phi_4 \frac{B}{K} + \phi_5 \frac{W}{K} + \phi_6 \frac{R}{K}}{1 + \zeta_4 \frac{B}{K} + \zeta_5 \frac{W}{K} + \zeta_6 \frac{R}{K}} - \frac{L}{\tau_L}, \tag{4}$$

$$\frac{dN^b}{dt} = \frac{\beta_{N^b} L^{\text{trans}}}{K + L^{\text{trans}}} - \frac{N^b}{\tau_{N^b}}. \tag{5}$$

Here, the parameters β_{L,N^b} and τ_{L,N^b} correspond to the maximum growth rates and mean lifetimes for the ligand and NICD, respectively. The binding of Notch receptors of a cell to corresponding ligands of neighboring cells (L^{trans}) causes the receptor's intracellular domain (N^b) to be released and translocated to the nucleus [40]. We consider Notch and the patterning genes to regulate the expression of each other [see Fig. 1(b)]. Specifically, we consider four classes of intercellular interactions based on whether NICD up or downregulates the expression of B, W, and R genes, and whether Notch ligand production is promoted or repressed by the patterning genes (mirroring the response of the ligands Jagged and Delta, respectively [41–43]). For simplicity, the ligand is assumed to be either activated by all the genes or inhibited by each of them, while the genes themselves are regulated by NICD in

a qualitatively identical manner [44]. Thus, the four classes of intercellular coupling, defined by up (G^+) or downregulation (G^-) of the patterning genes, and promotion (L^+) or repression (L^-) of the ligand, and specified by the parameter set ($\varphi_i, \xi_i, \phi_j, \zeta_j$), correspond to type I: G^-, L^- $(0, \theta_i, 0, \theta_j)$; type II: G^-, L^+ $(0, \theta_i, \theta_j, 1)$; type III: G^+, L^- $(\theta_i, 1, 0, \theta_j)$; and type IV: G^+, L^+ $(\theta_i, 1, \theta_j, 1)$, where $i = 1, 2, 3$ and $j = 4, 5, 6$.

We choose values for the parameters such that the absence of coupling (i.e., $\varphi_i = 0$, $\xi_i = 0$, $\forall i$) yields an idealized flag with three chromatic regions of equal length, each corresponding to distinct cell fates [45]. To see how Notch signaling between adjacent cells can alter the ordered pattern of cells having different fates, even when the morphogen gradient and the parameters of the interpretation module are kept unchanged, we systematically investigate the six-dimensional parameter space spanned by $\Theta = \{\theta_1, \theta_2, \theta_3, \theta_4, \theta_5, \theta_6\}$. For each of the four types of coupling described above, we consider 10^5 realizations of the model obtained by randomly sampling Θ. Each of the parameters $\theta_{1,\ldots,6}$ is sampled from the interval [1,10] (for G^+ and L^+) or [0.1,1.0] (for G^- and L^-). Altering the nature and strength of intercellular interactions, we observe a diversity of resulting patterns of distinct cell fates that differ from the flag obtained in the uncoupled case not only in terms of the lengths of the individual chromatic regions, but also in terms of their number and sequential order. To quantify the variation in the flags obtained from the different realizations, we characterize them by (i) the number n_B of fate boundaries, which are defined by adjacent cells having different fates, and (ii) a Hamming distance d_H to the idealized flag (obtained in the absence of coupling), determined by enumerating the number of cells whose fates are different in the two flags. Depending on whether NICD up or downregulates the expression of the patterning genes, we obtain two qualitatively different outcomes. While repression of B, W, R almost always results in flags having two boundaries [Figs. 2(a) and 2(b)], promoting their expression yields a much wider range of n_B [Figs. 2(c) and 2(d)]. Furthermore, the flags generated for coupling types I and II are typically closer (in terms of d_H) to the idealized flag as compared to types III and IV. We note that these results are not qualitatively altered upon introducing stochastic fluctuations in the morphogen concentration and/or the variables B, W, R, L, N^b describing the system dynamics [45].

In contrast to the parameters governing the regulation of B, W, and R by NICD, those associated with modulating the effect of the patterning genes on ligand production appear to have little or no effect on the resulting flags. We use a variance-based sensitivity analysis technique to quantify the contribution of each of these parameters in determining the cell fates [46]. We consider the final state of each cell i comprising the domain to be represented by a discrete scalar variable $F_i \in \{0, 1, 2\}$ corresponding to blue, white, and red. Prior to quantifying the role played by the parameters Θ at each cell, we quantify the variance (σ^2) in the fate F_i across the different realizations [Figs. 3(a) to 3(d), upper panels]. For coupling types I and II, we note that σ^2 is negligible throughout the array, except around the location of the two fate boundaries in the idealized flag. In contrast, σ^2 has a finite value at all locations in coupling types III and IV. The

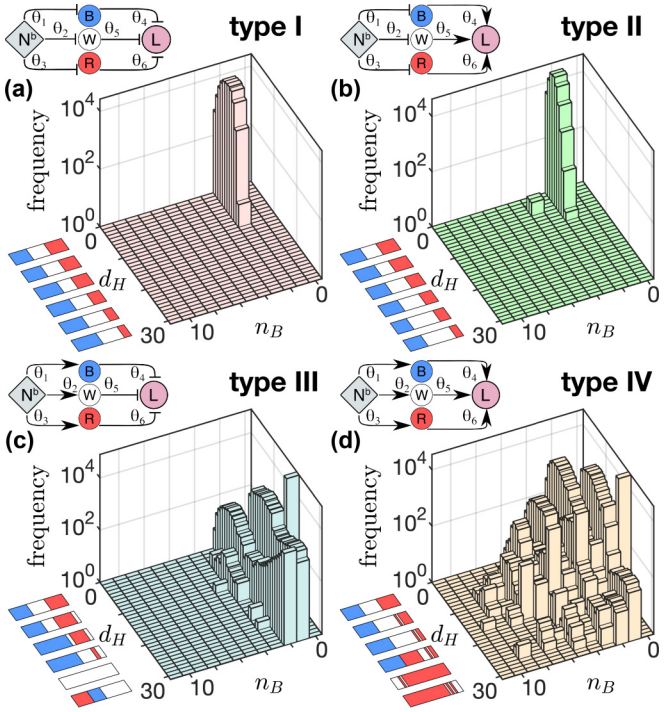

FIG. 2. The diversity in the spatial patterns of cell fates is controlled by the nature of interactions underlying Notch-mediated intercellular coupling. The intercellular interactions can be classified into four types, determined by whether NICD up or downregulates the patterning genes, and in turn, the genes up or downregulate ligand production, represented by the four motifs in the upper left corners in (a)–(d) [arrows representing up/downregulation are as indicated in Fig. 1(b)]. For each type, the frequency distributions of different flags, i.e., patterns representing the sequential arrangement of distinct cell fates, are obtained by randomly sampling $\theta_{1,\ldots,6}$, are shown in (a)–(d) for a 1D domain comprising 30 cells subject to the morphogen gradient shown in Fig. 1(c). In the absence of intercellular coupling, the domain is divided into three equal segments of cells having different fates [as in Fig. 1(d)]. The flags obtained upon coupling the cells are characterized by the number of fate boundaries n_B and the difference d_H with the pattern in the uncoupled system (which has equal chromatic divisions). For types I, II (where NICD downregulates B, W, and R) almost all flags have the same chromatic order and n_B as the idealized flag shown in Fig. 1 (a, left), with d_H limited to very low values [(a) and (b), cf. Fig. 1 (a, right, top row)]. In contrast, the flags seen for types III, IV (where NICD upregulates B, W, and R) exhibit large variation from the uncoupled case in terms of both d_H and n_B [(c) and (d), cf. Fig. 1 (a, right, bottom row)]. For each type, sample flags are displayed in ascending order of d_H along the corresponding axis.

contribution of the different parameters $\theta_{1,\ldots,6}$ to the observed variation in the fate of each cell is measured by the respective first-order sensitivity indices $S1$, expressed as the variance of $\langle F_i|\theta_j\rangle_{\theta_{k(\neq j)}}$ normalized by σ^2 [45]. Figures 3(a) to 3(d), lower panels, show that only θ_2 and θ_3 contribute significantly in all coupling types, while for coupling types III and IV, θ_1 also plays an important role. We note that the bulk of the variation in F_i can be explained by $S1$ alone, suggesting that the observed diversity can be largely explained in terms of the independent actions of each parameter.

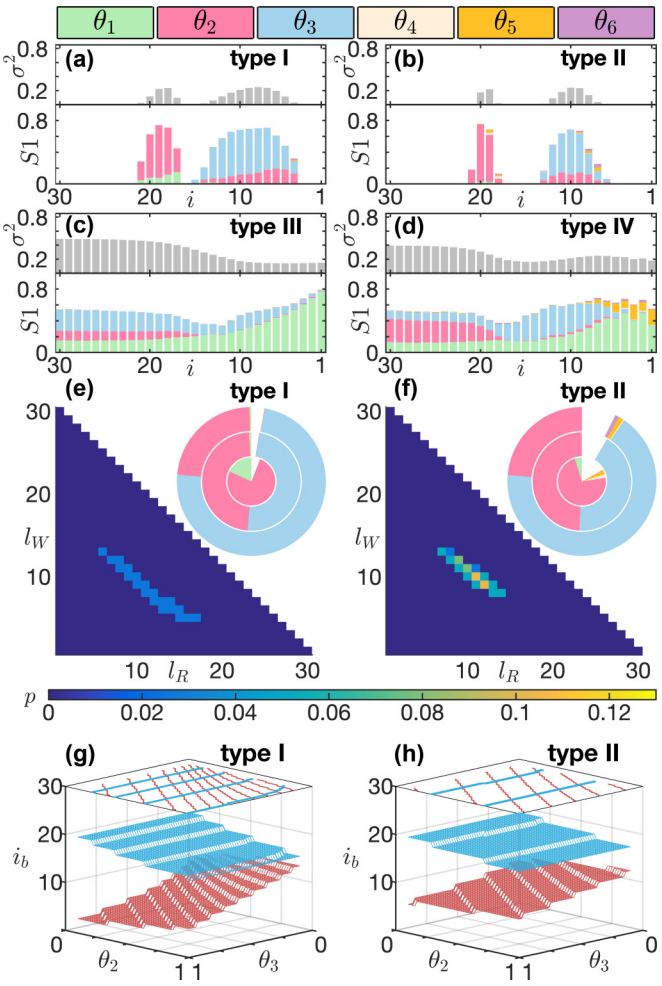

FIG. 3. Sensitivity of the flags to intercellular coupling parameters. (a)–(d) Dependence of the variation in cell fates on the spatial location i of each cell in a 1D domain, as well as, the differential contributions of the coupling parameters Θ to the variation, for the four types of Notch-mediated interactions. The top half of each panel shows the variance σ^2 of the discrete variable representing the three possible fates (blue, white, red) that a cell can attain. The bottom halves display the fraction of the variance that can be accounted for by independently varying each of the parameters (colored according to the legend), as quantified by the first order sensitivity index $S1$. (a, b) When NICD downregulates the patterning genes, most of the variation is localized around the two fate boundaries of the uncoupled case and is sensitive to changes in θ_2 and θ_3. In contrast, (c, d) variation is seen across the domain when NICD upregulates the genes, with most of the contribution from θ_1, θ_2, and θ_3. (e, f) Focusing on types I, II for which chromatic order and n_B of the flags are invariant, we observe that the lengths of the red and white segments (l_R and l_W, respectively) are narrowly distributed around those in the uncoupled case ($l_R^* = 10$, $l_W^* = 10$). The sensitivity of the segment lengths to the parameters Θ are shown in the concentric piecharts (outer: l_R, middle: l_W, inner: l_B). (g, h) The dependence of the location i_b of the two fate boundaries (shown in blue and red, respectively) on the parameters θ_2 and θ_3, with contour lines shown at the top.

As flags that do not conserve n_B or the chromatic order of the idealized flag represent pronounced aberrations that are undesirable in the context of development, we focus on coupling types I and II, which are extremely unlikely to generate such flags. Indeed, the localization of variation in cell fates for these coupling types is consistent with the resulting flags typically having low d_H (see Fig. 2). Moreover, almost all of them have $n_B = 2$, which allows the flags to be uniquely specified by the lengths of any two out of the three chromatic regions. Figures 3(e) and 3(f) show that the joint distribution of the lengths l_R, l_W of the regions having red and white fates, respectively, is concentrated around that of the flag obtained in absence of coupling (viz., $l_R = l_W = 10$ for an array of 30 cells) for both coupling types. The outer, middle, and inner rings in the adjoining piecharts represent the contribution of each parameter $\theta_{1,\ldots,6}$ to the variation observed in l_R, l_W, and l_B, respectively. This is quantified by the corresponding first-order sensitivity indices, expressed in terms of the angles subtended by each of the colored segments representing the different parameters. Note that the bulk of the observed variance in the lengths can be attributed to changes in each of the parameters, independent of the others. As θ_2 and θ_3 appear to be almost exclusively responsible for the observed variation in the flags, in Fig. 3(g) and 3(h) we explicitly show how the locations of the two boundaries i_b between R, W (red) and W, B (blue) change on varying these two parameters. For both coupling types, increasing θ_2 is observed to expand both the red and blue region at the expense of the white region in the middle, while increasing θ_3 results in reduction of the red region but with little impact on the W-B boundary. Thus, the variation in the flags resulting from down-regulation by NICD of the genes forming the morphogen interpretation module can be explained by using only a pair of parameters controlling the repression of W and R genes, respectively. The predicted alterations in the resulting flag upon changing Notch expression can be tested experimentally to validate the role of intercellular interactions in determining the spatial pattern of cell fates outlined here. Intuitively, the direct role of NICD in regulating the expression of the patterning genes, which in turn determine the cell fate patterns, explains the relative importance of these interactions (G^+, G^-) compared to those between the genes and the ligand (L^+, L^-). Furthermore, as these last are convergent, variations in θ_4, θ_5, and θ_6 can mutually compensate each other, ensuring that the pattern is relatively robust with respect to these interactions.

To conclude, our work reveals that juxtacrine signaling between cells could play a key role in adaptively regulating cellular differentiation that results in morphogenesis. While the diffusing morphogen sets up a global field that triggers the breaking of the intrinsic symmetry, and the gene regulatory circuit translates the local morphogen concentration into the eventual cell fates, the intercellular interactions allow information from the environment of each cell to be incorporated into the process. Apart from their utility in correcting for fluctuations in the signal in the presence of noise [29], such an intermediate-scale process can increase the robustness of the system in generating the desired flag by compensating for mutations affecting the production and/or interpretation of the morphogen. We show this by using a modeling approach that integrates two apparently disparate paradigms for investigating biological pattern formation [31], namely, that of boundary-organized mechanisms involving a prepattern such as a morphogen concentration gradient and self-organized mechanisms involving interactions between constituents [50].

ACKNOWLEDGMENTS

We would like to thank James P. Sethna and Marcin Zagórski for helpful discussions. S.N.M. has been supported by the IMSc Complex Systems Project (12th Plan), and the Center of Excellence in Complex Systems and Data Science, both funded by the Department of Atomic Energy, Government of India. The simulations required for this work were supported by IMSc High Performance Computing facility (hpc.imsc.res.in) [Nandadevi].

[1] M. C. Cross and P. C. Hohenberg, Rev. Mod. Phys. **65**, 851 (1993).
[2] A. J. Koch and H. Meinhardt, Rev. Mod. Phys. **66**, 1481 (1994).
[3] P. Ball, *The Self-Made Tapestry: Pattern Formation in Nature* (Oxford University Press, Oxford, 1999).
[4] H. T. Zhang and T. Hiiragi, Annu. Rev. Cell Dev. Biol. **34**, 405 (2018).
[5] A. M. Turing, Philos. Trans. R. Soc. London **237**, 37 (1952).
[6] H. Meinhardt, *Models of Biological Pattern Formation* (Academic, London, 1982).
[7] S. Werner, T. Stückemann, M. Beirán Amigo, J. C. Rink, F. Jülicher, and B. M. Friedrich, Phys. Rev. Lett. **114**, 138101 (2015).
[8] L. Wolpert, J. Theor. Biol. **25**, 1 (1969).
[9] L. Wolpert, Development **107**, 3 (1989).
[10] J. Sharpe, Development, **146**, dev185967 (2019).
[11] F. Crick, Nature (London) **225**, 420 (1970).
[12] W. Driever and C. Nüsslein-Volhard, Cell **54**, 95 (1988).
[13] A. A. Teleman, M. Strigini, and S. M. Cohen, Cell **105**, 559 (2001).
[14] A. D. Lander, Q. Nie, and F. Y. M. Wan, Dev. Cell **2**, 785 (2002).
[15] A. D. Lander, Cell **128**, 245 (2007).
[16] T. Bollenbach, K. Kruse, P. Pantazis, M. González-Gaitán, and F. Jülicher, Phys. Rev. Lett. **94**, 018103 (2005).
[17] J. L. England and J. Cardy, Phys. Rev. Lett. **94**, 078101 (2005).
[18] G. Hornung, B. Berkowitz, and N. Barkai, Phys. Rev. E **72**, 041916 (2005).
[19] D. Ben-Zvi and N. Barkai, Proc. Natl. Acad. Sci. USA **107**, 6924 (2010).
[20] S. B. Yuste, E. Abad, and K. Lindenberg, Phys. Rev. E **82**, 061123 (2010).
[21] C. B. Muratov, P. V. Gordon, and S. Y. Shvartsman, Phys. Rev. E **84**, 041916 (2011).
[22] J. B. Gurdon and P.-Y. Bourillot, Nature (London) **413**, 797 (2001).
[23] H. L. Ashe and J. Briscoe, Development **133**, 385 (2006).
[24] K. W. Rogers and A. F. Schier, Annu. Rev. Cell Dev. Biol. **27**, 377 (2011).
[25] S. F. Gilbert, *Developmental Biology* (Sinauer, Sunderland, MA, 2013).
[26] J. H. Kong, L. Yang, E. Dessaud, K. Chuang, D. M. Moore, R. Rohatgi, J. Briscoe, and B. G. Novitch, Dev. Cell **33**, 373 (2015).
[27] S. Artavanis-Tsakonas, M. D. Rand, and R. J. Lake, Science **284**, 770 (1999).
[28] R. Kopan and M. X. G. Ilagan, Cell **137**, 216 (2009).
[29] D. Sprinzak, A. Lakhanpal, L. LeBon, J. Garcia-Ojalvo, and M. B. Elowitz, PLoS Comput. Biol. **7**, e1002069 (2011).
[30] T. Erdmann, M. Howard, and P. R. ten Wolde, Phys. Rev. Lett. **103**, 258101 (2009).
[31] A. D. Lander, Cell **144**, 955 (2011).
[32] A. D. Lander, Science **339**, 923 (2013).
[33] K. Exelby, E. Herrera-Delgado, L. G. Perez, R. Perez-Carrasco, A. Sagner, V. Metzis, P. Sollich, and J. Briscoe, Development **148**, dev197566 (2021).
[34] The feedback loop arises from the Notch intracellular domain (NICD) of a cell i controlling the production of NICD in the neighboring cell j by affecting the production of the corresponding ligand in cell i, which in turn results in NICD of j controlling that of i, thereby completing the loop.
[35] E. Dessaud, A. P. McMahon, and J. Briscoe, Development **135**, 2489 (2008).
[36] E. Dessaud, V. Ribes, N. Balaskas, L. L. Yang, A. Pierani, A. Kicheva, B. G. Novitch, J. Briscoe, and N. Sasai, PLoS Biol. **8**, e1000382 (2010).
[37] N. Balaskas, A. Ribeiro, J. Panovska, E. Dessaud, N. Sasai, K. M. Page, J. Briscoe, and V. Ribes, Cell **148**, 273 (2012).
[38] Y. Dang, D. A. J. Grundel, and H. Youk, Cell Syst. **10**, 82 (2020).
[39] We assume that the concentration of morphogens across the domain is implicitly set by a spatially uniform linear synthesis-diffusion-degradation (SDD) model, which yields an exponential gradient in the morphogen concentration M at its steady state. We assume that S_M is a proxy for the concentration of the signaling molecule that is triggered when morphogen molecules bind successfully with the cell membrane receptors.
[40] We assume the number of receptors in each cell to be sufficiently high such that saturation is not reached.
[41] H. Shimojo, T. Ohtsuka, and R. Kageyama, Front. Neurosci. **5**, 78 (2011).
[42] L. J. Manderfield, F. A. High, K. A. Engleka, F. Liu, L. Li, S. Rentschler, and J. A. Epstein, Circulation **125**, 323 (2012).
[43] M. Boareto, M. K. Jolly, M. Lu, J. N. Onuchic, C. Clementi, and E. Ben-Jacob, Proc. Natl. Acad. Sci. USA **112**, E402 (2015).
[44] While the results reported here are under the simplifying assumption that the patterning genes are either all upregulated or downregulated by NICD, we explicitly verified that the results are qualitatively unchanged when we individually alter the nature of interactions that are chosen on the basis of the sensitivity analysis. See Supplemental Material at http://link.aps.org/supplemental/10.1103/PhysRevE.103.062409 for details.
[45] See Supplemental Material at http://link.aps.org/supplemental/10.1103/PhysRevE.103.062409 for details, which includes Refs. [46–49].
[46] A. Saltelli and I. M. Sobol', Matem. Mod. **7**, 16 (1995).
[47] K. S. Brown and J. P. Sethna, Phys. Rev. E **68**, 021904 (2003).
[48] J. J. Waterfall, F. P. Casey, R. N. Gutenkunst, K. S. Brown, C. R. Myers, P. W. Brouwer, V. Elser, and J. P. Sethna, Phys. Rev. Lett. **97**, 150601 (2006).
[49] R. N. Gutenkunst, J. J. Waterfall, F. P. Casey, K. S. Brown, C. R. Myers, and J. P. Sethna, PLoS Comput. Biol. **3**, e189 (2007).
[50] J. B. A. Green and J. Sharpe, Development **142**, 1203 (2015).